



Growth of Convection and Boundary Layers in Binary Mixtures

C. Fütterer and M. Lücke

Institut für Theoretische Physik, Universität des Saarlandes
Postfach 151150, D-66041 Saarbrücken, Germany

In binary mixtures exposed to gravitation and a large enough temperature gradient a complicated transition occurs from a pure heat-conducting to a convective state. During this transition, the spatiotemporal behaviour of the concentration field in the bulk of the layer and close to the boundaries varies dramatically, which is the main issue of this publication. © 2000 Elsevier Science B.V. All rights reserved.

1. INTRODUCTION

Convection in binary miscible fluids like ethanol - water, $^3\text{He} - ^4\text{He}$, or solutions of salt in water shows many additional phenomena in comparison to convection in simple fluid. It displays interesting properties like a subcritical bifurcation (hysteresis), oscillatory instabilities, stationary states, boundary layers – the subject of this publication, complex spatiotemporal behaviour, and turbulence [1, 2, 3]. It is a paradigmatic system for research on systems far from equilibrium because the equations are well-known, the experiments are sufficiently simple, and computing power is strong enough to perform simulations on a macroscopic scale. On the other hand, it is also of great practical interest: most fluids in nature are mixtures.

We use a finite-difference algorithm to solve the hydrodynamic field equations in a two dimensional convection-cell of height d and length $2d$ with realistic horizontal and periodic lateral boundary conditions. The x-axis is parallel and the z-axis is perpendicular to the horizontal boundaries. We scale length in units of the layer thickness d and time in units of the thermal-diffusion time d^2/κ as in e.g. [3] or [4]. Parameters are the Prandtl number $\sigma = \nu/\kappa = 10$, that is the ratio of velocity diffusion over temperature diffusion, the Lewis number $L = D/\kappa = 0.01$, that is the ratio of concentration diffusion over temperature diffusion, and the Soret number $\psi = -0.25$ which measures the coupling of the temperature field into the concentration equation. The concentration diffusion is much smaller than the thermal diffusion and causes a long time decay of concentration variations. The control parameter is the reduced Rayleigh number r that is the quotient

of the Rayleigh number R and the critical Rayleigh number of the pure fluid $R_c(\psi = 0)$. It controls the temperature difference between the upper and lower plate which enforces

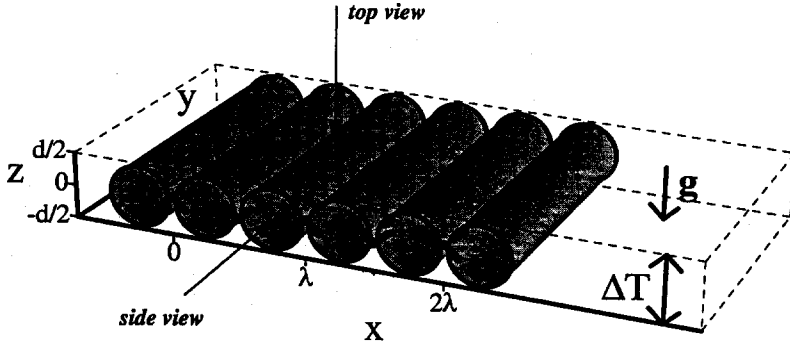


Figure 1: The Rayleigh Bénard System is a box filled with a fluid. It is heated from below and cooled from above. The temperature difference is ΔT . At the bottom ($z = -d/2$) and at the top ($z = d/2$) there are two perfectly heat-conducting plates. The gravitational acceleration g results in a buoyancy force. If surpassing a certain temperature difference between the plates, the convective roll structure with the wavelength λ emerges.

a heat flow and drives the system out of equilibrium. We use a small supercritical value $r = 1.42$ that is about 6.2% beyond the critical value of the onset of convection in the binary mixture, $r_c = 1.3348$.

For these parameters the pure fluid shows exponentially growing convection that saturates in stationary-convection rolls. Convection in binary mixtures on the other hand shows for the mentioned parameters exponentially and oscillatory growing standing-waves (SWs) and ends with travelling-waves (TWs). The Soret coupling is the reason for this oscillatory behaviour [1, 5].

This paper investigates the behaviour of the bulk fluid and of the boundary layer during the growth of convection and the nonlinear transition. In our system of length $\Gamma = 2$ with periodic lateral boundary conditions, only lateral wave numbers which are multiples of $k = 2\pi/\Gamma$ appear. Thus defects, grain boundaries, and large scale modulations are suppressed.

2. CONVECTION GROWTH – TOP VIEW SHADOWGRAPH

For a small enough temperature difference $r < r_c$ the fields in the conductive state are

$$T(x, z) = -z \quad \text{and} \quad w(x, z) = 0 \quad C(x, z) = -\psi z \quad (1)$$

and this "ground-state" is the starting-point for the computer simulations discussed here. When increasing the temperature difference above the critical value $r > r_c$, convection begins to grow out of the ground-state if the latter is slightly perturbed by noise.

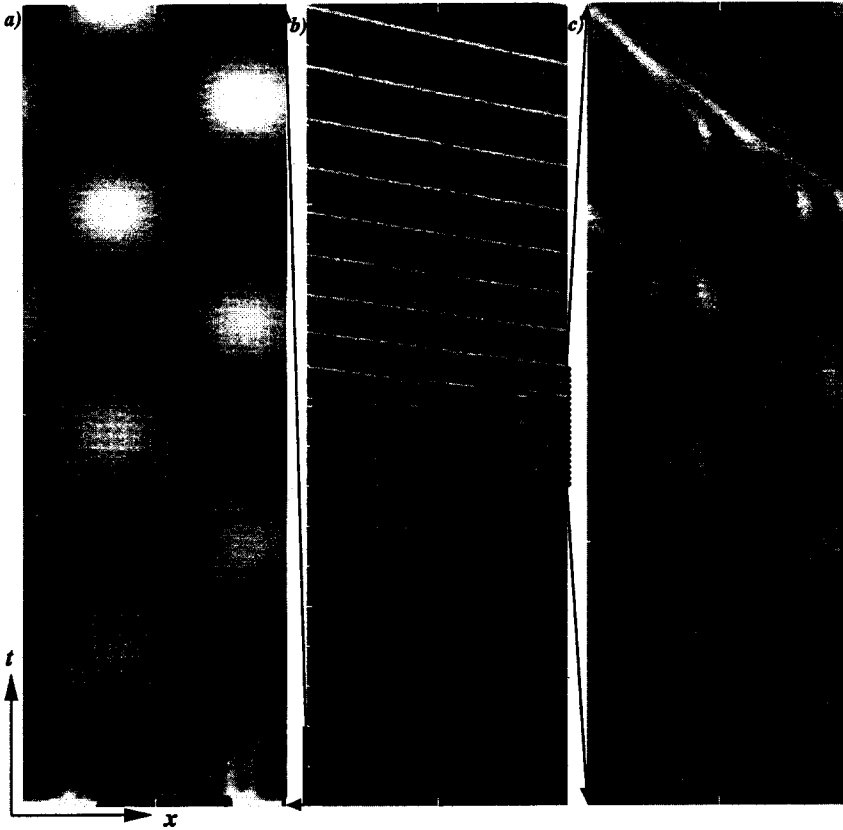


Figure 2: Space-time plot of the top-view shadowgraph of temporal evolution. Initial condition is the conductive state with small noise (close to the experimental situation). In b) the whole range $t = 0 - 20$ is presented. In a) the interval $t = 0 - 2$ of the linear growing, and in c) the interval $t = 8 - 11$ of the nonlinear mixing phase is enlarged. The distance between two tick-marks represents one time unit. Along the spatial axis one wavelength of the pattern is shown. The horizontal tick marks label the time units. The arrows between the three images indicate the enlarged sections.

In Fig. 2 the experimentally relevant "shadowgraph" of the evolution is shown. In experiments, the shadowgraph is obtained by transmitting light from the top through the fluid. The light is reflected at the polished bottom plate and collected on the top along a line parallel to the x-axis. Due to density variations caused by temperature *and* concentration differences, the light-beams are focused or defocused in the fluid and give

an image of the pattern in the observed intensity. Small density variations allow a linear expansion [8, 9]

$$I(x, t) \sim \langle \partial_x^2 C(x, z, t) - 0.919 \partial_x^2 T(x, z, t) \rangle_z .$$

Thus the shadowgraph can also be calculated from simulation data and compared with experiments.

In Fig. 2b) the range $t = 0, \dots, 20$ of the evolution is displayed. The initial behaviour is shown on the left in a) and the transition from SW to TW at $t \approx 10.3$ is given in c). After a short initial transient that depends strongly on the noisy initial condition the lateral harmonic critical modes dominate the system in a). These two critical modes represent two counterpropagating TWs. They form a SW if their amplitudes are of almost equal strength. In c) the leftgoing TW disappears within a very short time and the concentration field gets strongly anharmonic. Therefore the shadowgraph changes from oscillations to slanted stripes and sharp variations that indicates propagation of the pattern. The sharp variations reflect the strong anharmonic TW profiles of the concentration entering into $I(x, t)$. After that phase the slope of the stripes in Fig. 2b) increases slightly with time since the velocity of the TW decreases slowly.

3. SIDE VIEW PICTURES OF THE CONCENTRATION DYNAMICS

What happens to the convection structures during the transition from a standing to a travelling wave as we found in the preceding chapter? Fig. 3 presents a selection of *side view* snapshots of the evolution of the concentration field and reveals the complicated mixing dynamics that was hidden in Fig. 2. Isolines and gray-levels represent the concentration field and streamlines are plotted as dotted lines. Furthermore an overview with a detailed plot of the modulus of the first lateral Fourier coefficient (first LFCM) at the midplane $z = 0$ as well as between the midplane and the boundary at $z = -1/4$ ("intermediate layer") is included.

Small erratic perturbations of the conductive state shown in a) lead to a standing wave in b). The concentration isolines are mostly curved in the middle region and the first LFCM at $z = 0$ oscillates more than at $z = -1/4$, because the destabilization is stronger in the bulk fluid. The streamlines are also shown in the snapshots. If the advection dominates the dynamics as it is the case in b) - h), the concentration field follows the streamlines almost passively. While the streamlines bend the concentration-isolines increasingly, the concentration field becomes more and more anharmonic in c). The anharmonic structure in Fig. 2c) results in large higher lateral Fourier modes.

The small phase shift between the concentration field and the streamlines in Fig. 3b) is thereafter strongly amplified in c), d), etc. Since the regions of maximal concentration in d) coincide with the centres of the streamlines the yet growing "concentration fingers" are bent to the right in e). This process corresponds to the transition to the left-going TW in Fig. 2 at $t \approx 10.3$. In fact in the bulk the concentration structure remains at the same place from b) to f). Close to the boundaries in the intermediate plane the stem of the concentration jet moves to the left while its upper part in the bulk and the "foot" close to the lower boundary lag behind. Consequently the structure is strongly bent sideways. After the "bending-sideways" phase [d), e)] the advection pushes the concentration field

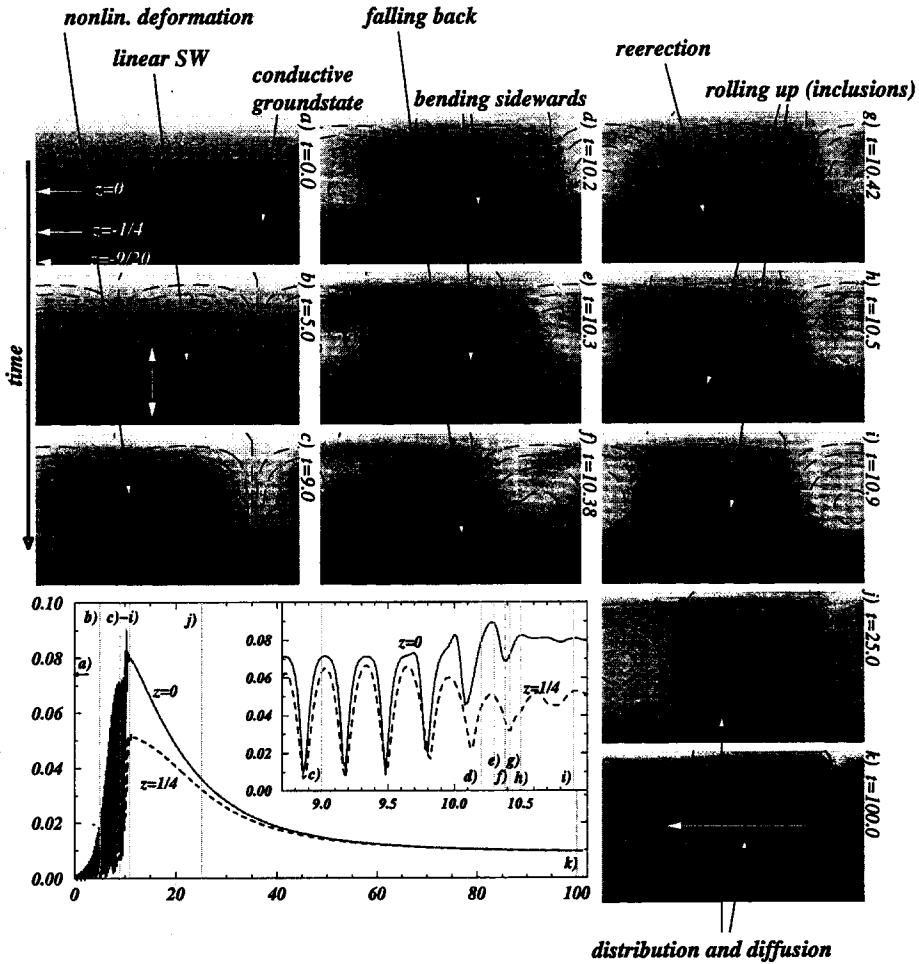


Figure 3: The concentration field shows a complicated mixing dynamics combined with the interaction of two counterpropagating travelling-waves. The values of the concentration-isolines can be read off in a) where the vertical profile is linear $C(x, z) = -\psi z$. Streamlines are shown by dotted lines. Beneath the dynamics of the first LFCM is depicted.

back to the boundaries in f). As a consequence the first LFCM at $z = 0$ shrinks in f), the phase at $z = -1/4$ makes a leap forwards to the left, and the whole pattern begins in g) to move to the left. The following dynamics shows the rolling and mixing up of the concentration field on a long time scale. The first LFCM decreases accordingly.

Side view pictures of transients in long systems have been observed in [7]. But large scale modulations and fronts greatly complicate the picture there.

4. AMPLITUDES AND PHASE DIFFERENCES

Subsequently, the observations of the preceding chapter as well as further details are discussed quantitatively. To that end the phase differences of the concentration, the temperature, and the velocity field between the bulk at $z = 0$ and at $z = -1/4$ [b]) as well as between the bulk at $z = 0$ and at $z = -9/20$ [c]) are presented in Fig. 4. The amplitudes in a) allow a rough comparison with Fig. 3. The initial state was prepared to be a pure right-moving TW. Since the counter-propagating wave is absent the amplitudes do not oscillate but the evolution of the TW at long times is the same as in Fig. 3. The phase relations are here much easier to analyse because they correspond directly to spatial rather than to temporal differences as it is the case for the SW.

Initially, all amplitudes grow exponentially in Fig. 4a) as determined by the linear stability analysis [6]. The point of inflection of the amplitudes at $t \approx 11.7$ puts an end to this exponential-growth phase and initiates the nonlinear phase. The concentration amplitude shows the largest overshooting at $z = 0$. Close to the boundaries ($z = -9/20$) it grows later and without overshooting. The amplitude dynamics of the concentration field is much slower and weaker here than at the other positions. Due to the vanishing velocity field at the boundaries the dynamics of the fluid in its vicinity slows down.

In Fig. 4c) all phase differences are initially negative. The structures in the boundary region follow the bulk region, accordingly. The fast oscillations that can be observed during the first 10 time units are numerical artefacts and should be ignored. At the point of inflection in a) that marks the beginning of the nonlinear domain both displayed phase differences begin to grow. At $t \approx 15$ they change the sign at the same time. From now on the phase of the fields in the boundary region moves ahead. During almost the whole dynamics, the phase difference of the concentration field shows much larger values than the one of the temperature field that are again stronger than the one of the velocity field. That reflects the hierarchy of the diffusion constants. The final phase shift $\varphi_{C_1}(z = 9/20) - \varphi_{C_1}(z = 0)$ is about $\pi/2$. The values of the velocity field are omitted because a too small amplitude at $z = -9/20$ prevents their proper calculation.

The phase differences in Fig. 4b) are generally much smaller than in c). As in c) they are initially negative. In contrast to the phase of the temperature and velocity field the concentration phase gets positive *before* the other phases and additionally *before* the inflection point. At the inflection point the velocity-field phase vanishes. At this point the concentration field is rolled up into a plateau and the phase difference of the concentration field becomes very large because only the stem connecting the boundary layer to the growing plateau [see Fig. 3h)] is captured at $z = -1/4$. At $z = 0$ the whole plateau contributes to the Fourier coefficient (see also discussion in the preceding chapter). Later the growing plateau also crosses the $z = -1/4$ -region and the phase difference decreases. Finally the phase difference grows slowly again up to $\pi/2$ at $z = 9/20$ due to the boundary layers and the layers between the plateaus that become increasingly dominant in comparison to the more and more diffusively mixed plateaus [see Fig. 3k)].

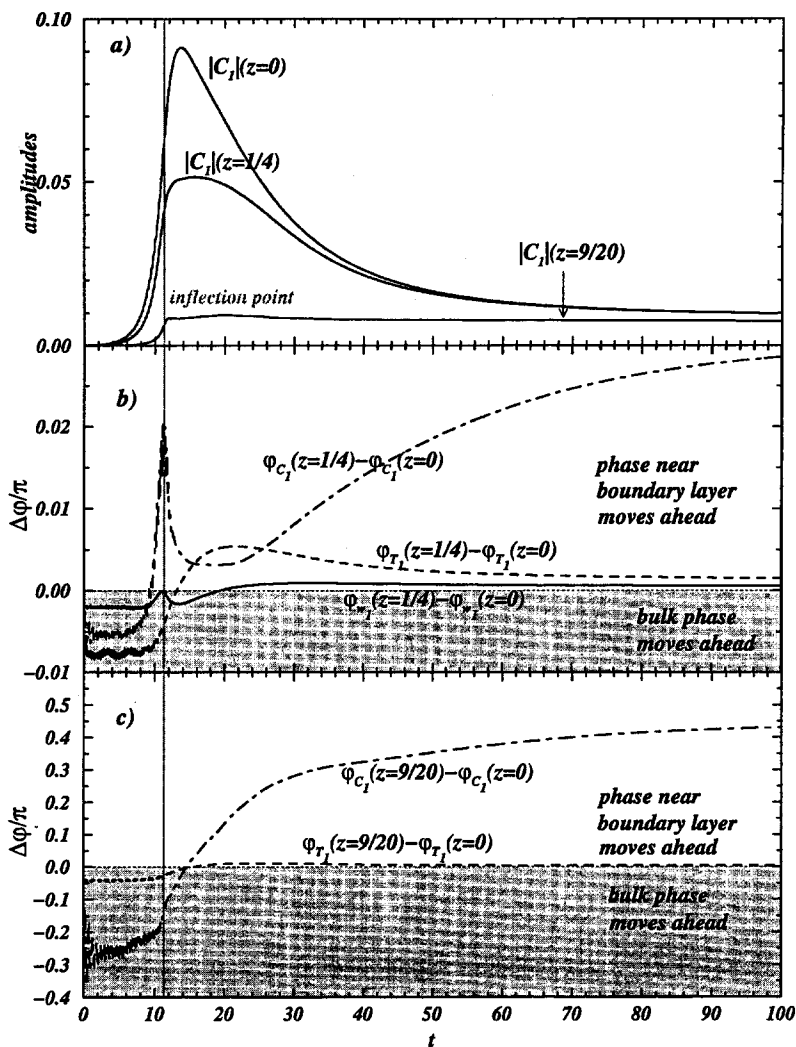


Figure 4: The amplitudes as well as the phase differences related to different z -positions $z = 0$, $z = -1/4$, and $z = -9/20$ are shown for a pure TW. The amplitude overshoots strongly at $z = 0$ but not at all at $z = -9/20$. All phase differences are initially negative and the bulk phase precedes in the evolution. Around the inflection point of the amplitude all phase differences become positive and the bulk phase lags behind the phases at other z positions.

5. CONCLUSION

We discussed the shadowgraph of the transition SW to TW starting from the slightly perturbed conductive ground-state. After a harmonic SW this transition is accompa-

nied by boundary layers that cause sharp structures. The side-view pictures revealed a complicated mixing dynamics that is responsible for the observations in the shadowgraph. During this process the amplitude of first lateral Fourier-mode of the concentration field at the midplane displayed a large overshooting. The amplitude dynamics at the boundaries was however much weaker. In the discussion of the transient phase differences we observed that first the phases at $z = 0$ preceded the phases at the boundary layer $z = -9/20$ and at the intermediate layer $z = -1/4$ while they lagged behind in the nonlinear phase. The concentration-phase difference $\varphi_{C_1}(z = -1/4) - \varphi_{C_1}(z = 0)$ shows a strong overshooting when passing the inflection point corresponding to the fast moving stem of the concentration finger. During almost the whole evolution the phase difference of the concentration field was much larger than that of the other fields.

References

- [1] M. C. Cross, P. C. Hohenberg, *Pattern Formation Outside of Equilibrium*, Rev. Mod. Phys. **65**, 851 (1993).
- [2] Structure and Dynamics of Nonlinear Convective States in Binary Fluid Mixtures, *Nonlinear Evolution of Spatio-Temporal Structures in Dissipative Continuous Systems*, edited by F. H. Busse, L. Kramer, NATO ASI Series B **225**, (Plenum, New York, 1990), p. 131.
- [3] W. Barten, M. Lücke, M. Kamps, R. Schmitz, *Convection in Binary Fluid Mixtures. I. Extended Traveling-Wave and Stationary States*, Phys. Rev. E **51**, 5636 (1995).
- [4] M. Lücke, W. Barten, P. Büchel, C. Fütterer, St. Hollinger, and Ch. Jung, *Structure and Dynamics of Nonlinear Convective States in Binary Fluid Mixtures*, submitted to *Evolution of Structures in Dissipative Continuous Systems*, edited by F. H. Busse, S. C. Müller, Lecture Note in Physics, (Springer).
- [5] J. K. Platten, J. C. Legros, *Convection in Liquids*, (Springer, Berlin, 1984).
- [6] W. Hort, Diplomarbeit (Saarbrücken, 1990);
- [7] B. L. Winkler, P. Kolodner, J. Fluid Mech. **240**, 31 (1992).
- [8] J. R. Jenkins, *Interpretation of shadowgraph pattern in Rayleigh-Bénard convection*, J. Fluid. Mech. **1900**, 451 (1988).
- [9] P. Kolodner, H. L. Williams, C. Moe, *Optical Measurement of the Soret Coefficient of Ethanol-Water Solutions*, J. Chem. Phys. **E55**, 6950 (1997).